Please cite this article as:

A. Szemjonov[a], M. Tasso[b], S. Ithurria[b], I. Ciofini[a], F. Labat[a], T. Pauporté*[a],

Ligand Exchange on CdSe Nanoplatelets for the Solar Light Sensitization of TiO_2 and ZnO Nanorod Arrays.

J. Photochem. Photobiol A, **2019**, *368*, 182–189. DOI: 10.1016/j.jphotochem.2018.09.042

[a] PSL Research University, Chimie ParisTech-CNRS, Institut de Recherche de Chimie Paris, UMR8247, 11 rue P. et M. Curie, 75005 Paris, France.

[b] Laboratoire de Physique et d'Etude des Matériaux, UMR 8213 du CNRS, ESPCI, 10 rue Vauquelin, 75231 Paris, France.

*Corresponding author. E-mail: thierry.pauporte@chimie-paristech.fr

Keywords: CdSe; Nanoplatelets; Ligand exchange; ZnO; TiO_2; Light sensitization

Abstract

In quantum dot (QD) solar cells, the *ex situ* sensitization of wide band gap semiconductors (WBSCs) makes it possible to control the shape and the passivation of the nanosized sensitizer. Hence, *ex situ* techniques can be used to investigate how the band gap of the sensitizers affects the performance of quantum dot solar cells. The latter can be precisely controlled in 1D confined structures such as quasi-2D nanoplatelets (NPLs), the thickness of which is defined with an atomic precision. In this work, we tested and thoroughly characterized the attachment of 7, 9 and 11 monolayers thick CdSe NPLs (as well as QDs for the sake of comparison) to ZnO and to TiO_2 nanorods. A crucial point of the *ex situ* techniques is the choice of bifunctional ligands that link the nanosized sensitizers to the WBSCs. Besides the well-known mercaptopropionic acid, we also studied two 'atomic linkers' (OH^- and SH^-) to minimize the distance between the sensitizer and the oxide. The as-prepared systems have been analyzed by UV/VIS absorption and Raman spectroscopy.

Among them, SH^- was found to be the most versatile linker that enabled the efficient attachment of all types of CdSe nanocrystals on ZnO and TiO_2 nanorods.

1. Introduction

In the last few years, quantum dots have attracted a great attention of the solar cell research community for their application as sensitizers to harvest light in photoelectrochemical[1,2] and photovoltaic solar cells.[3] QD sensitizers show several advantages such as a tunable absorption spectra [4] and the possibility of breaking the Shockley–Queisser efficiency limit of p–n junction photovoltaic solar cells [5] via multiple exciton generation (MEG) and hot carrier collection.[6] CdSe nanoparticles of different shapes, including QDs, have been widely used to efficiently sensitize ZnO and TiO_2 nanostructures for photovoltaic[7] and catalytic applications[8]. In a recent work, we have demonstrated the successful incorporation of quasi-two dimensional (2D) CdSe nanoplatelets (NPLs) into solar cells.[3] NPLs have also been proved to be useful for a broad range of applications ranging from single-photon sources[9] to biophotonics.[10] These systems show much narrower excitonic absorption and photoemission bands[11] and higher photoluminescence quantum yields than spherical QDs.[12] Moreover, the Auger recombination rate for these structures is around one order of magnitude smaller than in QDs.[13]

The first step of the preparation of *ex situ* NPL-sensitized solar cells is to find the right ligand that allows the attachment to the WBSC surface (typically TiO_2 or ZnO) and facilitates the transfer of the photoexcited electron between them. Therefore, the long oleate ($CH_3(CH_2)_7CH=CH(CH_2)_7COO^-$, noted OA^-) which is used as the passivating ligand of the CdSe nanoplatelets and spherical QDs surfaces during their preparation must be replaced by smaller and bifunctional ligands such as SH^-, OH^- and 3-mercaptopropionate

($HSCH_2CH_2CO_2^-$, noted MPA^-), one functional group (-SH for MPA^-) or valence electron (for SH^- and OH^-) is attached to the nanocrystal and the other one to the WBSC.

In the present paper, we investigate the sensitization of TiO_2 and ZnO nanorod (NR) structures by NPLs of various thicknesses controlled at the atomic monolayer scale and QDs functionalized by SH^-, OH^- and MPA^- ligands. The main characterization methods used in this study are UV-VIS and Raman spectroscopy. First, we present the characterization of the CdSe nanocrystals before and after ligand exchange, and then we analyze the CdSe-ligand-WBSC-NR heterostructures.

2. Experimental

2.1. Preparation of TiO_2 and ZnO nanorod arrays

The arrays of ZnO NRs were prepared on FTO/glass substrates as described in Ref. [3]. Their characterizations by SEM (Fig.S1), XRD (Fig.S2) and Raman spectroscopy (Fig.S3) are shown in Section A of the Supplementary Material. The synthesis of TiO_2 rutile nanorods was based on a previous work by Kim et al. [14]. The FTO-coated TEC 15 glasses were thoroughly cleaned first by a detergent and rinsed with deionized (DI) water. They were subsequently sonicated for 15 min in ethanol and for 15 min in acetone. Then, they were spin-coated with a 0.15 M titanium (IV) diisopropoxide bis(acetylacetonate) (denoted as TIPA) solution in butanol, and heated at 125 °C for 5 min. After the spin-coated film cooled down to room temperature, this procedure was repeated twice using a 0.30 M solution. The layers were then annealed at 500 °C for 15 min in a furnace. The nanorods were grown on the as-prepared seed layer in a stainless-steel autoclave with a Teflon liner. The growth solution was prepared by mixing 20 mL of deionized water with 20 mL of 37% hydrochloric acid, and then by adding 0.7 mL of titanium (IV) n-butoxide dropwise. The substrates were positioned at an angle of 45° with the seed layer facing against the wall of the Teflon liner. The autoclave was placed for 3 hours in an oven heated at 170 °C and let to cool down. The samples were

subsequently rinsed with deionized water, dried and annealed at 450°C for 1h. The characterizations of the TiO_2 NR arrays by SEM (Fig.S4), XRD (Fig.S5) and Raman spectroscopy (Fig.S6) are detailed in Section B of the Supplementary Material.

2.2 Nanoplatelets preparation and ligand exchange

7, 9 and 11 monolayers (MLs) thick CdSe NPLs were synthesized by following the procedures described in ref. [15], [16] and [12], respectively. In more detail, for the synthesis of 7 MLs thick NPLs, 240 mg $Cd(OAc)_2 \cdot 2H_2O$, 150 µL of OA and 12 mL of octadecene (ODE) were degassed in a three-neck flask under vacuum flow at 90 °C for 1 hour. The mixture was then heated to 190 °C under argon flow. When this temperature was reached, 150 µL of 1M trioctylphosphine selenide (TOP-Se), was injected, and the synthesis was continued at this temperature for 40 minutes. Finally, the mixture was quenched, and 2mL of OA and 30 mL of hexane were added. The NPLs were separated by centrifugation and re-suspended in 30 mL of hexane. In order to obtain 9MLs thick NPLs, an initial reaction mixture of 0.3 mL of cadmium myristate [$Cd(myr)_2$], 0.15 mmol Se powder and 10 mL of ODE was degassed at room temperature for ~20 minutes in a three-neck flask. Then, under argon flow, the temperature was set to 240 °C. When the mixture color turned orange (at around 200 °C), 0.2 mmol of $Cd(Ac)_2 \cdot 2H_2O$ was introduced through a neck. After 5 minutes at 240 °C, the mixture was quenched, and 2 mL of OA and 35 mL of hexane were added. The NPLs were separated by centrifugation and re-suspended in 10 mL of hexane. For the synthesis of 11 MLs thick NPLs, 0.3 mmol of $Cd(myr)_2$ and 10 mL of ODE were degassed for 20 minutes in a three neck flask. Then, under argon flow, the mixture was heated up to 240 °C and a suspension of 0.15 mmol of selenium mesh sonicated in 1 mL ODE was injected. After 1 minute, 0.4 mmol of $Cd(Ac)_2 \cdot 2H_2O$ was introduced through a neck. After 10 minutes at 240 °C, the mixture was quenched and 2 mL of OA and 35 mL of hexane were added. The NPLs were separated by centrifugation and were re-suspended in 10 mL of hexane. We

investigated these NPLs in detail, from both an experimental and theoretical points of view in our previous works [17-19]. TEM views of the NPL are shown in Figure S7 (Supplementary Material).

The synthesis protocol of QDs was based on Ref. [20]. Briefly, 0.4 mmol CdO powder, 1.2 mmol myristic acid (MA) and 10 mL ODE were introduced in a three neck flask, and degassed under Ar for 10 minutes. The mixture was heated up to 270 °C while strongly stirred. In the meantime, heterogeneous Se-ODE precursor was prepared by dissolving 0.4 mmol Se powder in 2 mL ODE. The mixture was sonicated for 15 minutes to disperse Se. When the temperature of 270 °C was reached, 1 mL of Se precursor solution was injected into the reaction mixture. Immediately after Se injection, the temperature was set to 260 °C. 8 minutes later, the reaction was stopped by cooling down the reaction mixture. The QDs were re-dispersed in 10 mL of toluene. Next, 10 mL isopropanol and 10 mL methanol were added, and the mixture was centrifuged at 5000 rpm for 7 minutes. After this cleaning step, QD precipitated as pellets at the bottom of the vial. The solution was discarded and the QDs re-dispersed in 10 mL of toluene. Next, 12 mmol OA was added to the QD pellets to replace the original myristic acid bounded to their surface. The purification step was repeated using methanol as a nonsolvent, and the OA-passivated QD pellets were re-suspended in toluene.

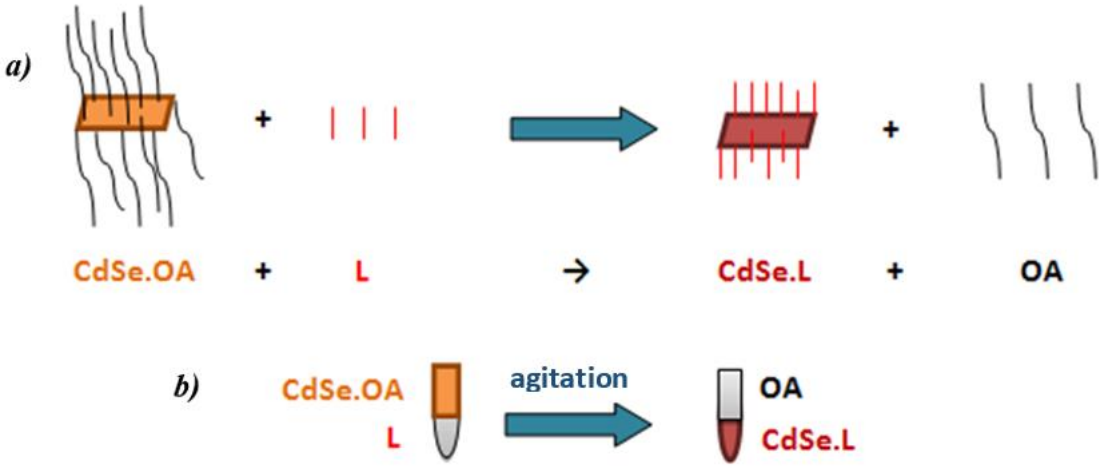

Scheme 1. a) Schematic illustration of biphasic ligands exchange reactions on CdSe NPLs. The short polar bifunctional linker is denoted as L. CdSe.OA and CdSe.L stand for CdSe NPLs passivated by OA and the L linker, respectively. b) Biphasic exchange transfer.

The OA^- ligands, passivating the (100) surface of the nanoplatelets, were exchanged to a hydrophilic ligand by a biphasic exchange reaction illustrated in Scheme 1. In the case of the OH^- and SH^- ligands, the exchange reactions were based on ref. [16]. The precursor solution of SH^- was prepared as follows. 0.1 mmol of NaSH was dissolved in 1 mL N-methylformamide (NMF) in a vial. For obtaining a OH^- precursor solution, 0.1 mmol of KOH was dissolved in 1 mL of NMF in a vial. Then, in a flask, 200 µL of the CdSe NPLs or QDs, 800 µL of hexane, 0.5 mL of NMF and 40 µL of the SH^- (respectively OH^-) precursor solution were stirred for 5 minutes. The NPLs were completely transferred from the non-polar to the polar phase due to the ligand exchange. These biphasic reactions are schematically illustrated in the Scheme 1. In the following, the as-prepared CdSe nanocrystals passivated by SH^- and OH^- ligands are denoted as CdSe.SH and CdSe.OH, respectively. In order to sensitize the ZnO or TiO_2 nanorod arrays, 50 µL of the CdSe.SH or CdSe.OH dispersion was dropcasted on the substrates. Then, they were heated at 150°C for 5 min to evaporate the NMF solvent. This temperature was low enough not to damage the structure of the CdSe nanocrystals. The sensitized samples are denoted as CdSe.SH–ZnO, CdSe.OH–ZnO, CdSe.SH–TiO_2 and CdSe.OH– TiO_2.

For the ligand exchange with MPA, 200 µL of MPA was added to 100 µL of CdSe NPLs dispersion in hexane in a vial, which was kept at 60°C for at least 6 hours. The resulting MPA-passivated NPLs were separated by centrifugation and re-suspended in NMF. They were rendered water-soluble by adding 2 mg of potassium tert-butoxide to deprotonate the carboxylate group of MPA. The NPLs were then precipitated in NMF. They were subsequently separated by centrifugation and re-dispersed in an aqueous solution with a basic pH to keep the carboxylate groups deprotonated. The pH of this aqueous solution was

adjusted to 13 by addition of mashed NaOH pellets. The as-prepared CdSe nanocrystals are denoted by CdSe.MPA in the following. The ZnO and TiO_2 nanorod arrays were sensitized by CdSe.MPA nanocrystals by drop-casting the basic aqueous dispersion of CdSe.MPA onto the substrates, similarly to the work published by Pan et al. [21]. Water was fully evaporated by leaving the samples in ambient air for 3h. The obtained sensitized samples are denoted as CdSe.MPA – ZnO and CdSe.MPA – TiO_2.

The absorption spectra of the samples were measured by a Varian Cary 5000 UV-VIS spectrophotometer. The Raman spectra were measured in air at ambient temperature (20 °C) using a confocal Renishaw inVia Reflex Raman spectroscope equipped with a 100x objective and a 473 nm blue laser. The samples were scanned 15 times at a laser power of 10% for an accumulation time of 30 seconds/scan. The data were collected and analyzed using the Renishaw's WiRE software.

3. Results and discussion

Quasi-2D nanostructures have step function-like absorption spectra with a high-intensity peak at each tread of a stair. As the latter is due to the creation of excitons in the quantum confined systems, these peaks are known as excitonic peaks. The absorption spectra of 3D-confined quantum dots also feature an excitonic peak structure due to the widening of discrete spectral lines, which is caused by heterodisperse QD size distribution and phonon-photon coupling. Changes in the shape and the position of excitonic peaks indicate structural changes in the nanocrystals, therefore their absorption spectra provide interesting insights into the functionalization of the nanocrystals, and on their subsequent attachment to ZnO or TiO_2 NRs. In the following, we only concentrate on the position of the first excitonic peak. It corresponds to the lowest electron excitation energy, [22] which is associated with the band gap energy of these nanocrystals.

3.1. Sensitization by SH^- functionalized NPL

The OA^- to SH^- ligand exchange changes the color of the NPL dispersions, which manifests in the redshift of the NPL excitonic peaks in the UV-VIS absorption spectra (Figure 1a). Due to quantum confinement effects, the bandgap of the NPLs (associated with the position of the first excitonic peak in this work) varies with the NPL thickness. Hence, the redshift is explained by the fact that ligand exchange results in the addition of a sulfide layer on the two Cd-rich (100) facets of the nanoplatelets. [3,16] The resulting sulfide-passivated NPLs can thus be regarded as quasi-(n+2) layers thick nanocrystals if they originally consisted of n atomic layers. This hypothesis is confirmed by the observation that the first excitonic peak of n layers thick CdSe.SH NPLs is approximately at the same wavelength as that of (n+2) layers thick CdSe.OA NPLs, indicating a similar degree of quantum confinement in the two systems. Another observable feature of the CdSe.SH absorption spectra is that their peaks are wider and less structured than those of the CdSe.OA NPLs. It suggests that the addition of sulfide layers distorts the CdSe NPL crystal structure.

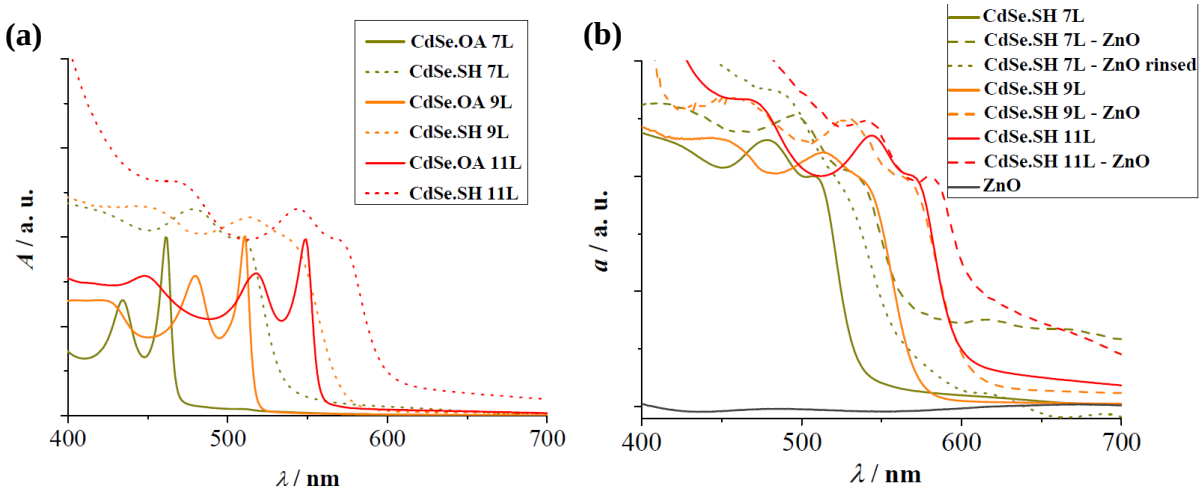

Figure 1. UV-VIS absorption spectra of (a) CdSe NPLs of different thicknesses (7, 9 and 11 layers). The NPLs passivated by OA are indicated in full lines, while NPLs after ligand exchange with SH^- are shown as dotted lines. (b)Spectra of the 7, 9 and 11 layers thick CdSe.SH NPLs in dispersion (indicated by green, orange and red full lines, respectively) and after attachment to ZnO nanorod arrays (indicated by dashed lines of the corresponding color, and by a dotted line after consequent washing with ethanol). Bare ZnO nanorod arrays are represented by a grey full line.

When attached to ZnO nanorods, the dispersion of CdSe.SH NPLs of all thicknesses formed a homogeneously colored layer on the ZnO substrate. The UV-VIS absorption spectra of these heterostructures are reported in Figure 1b, along with the UV-VIS absorption spectra of the bare NPLs for comparison. A redshift of the CdSe.SH NPLs excitonic peaks was observed for all NPL thicknesses considered in this study. This suggests that significant structural changes took place in the NPLs upon attachment to the ZnO nanorod arrays. To make sure that this shift was not the result of the aggregation of the NPLs on the ZnO substrate, the absorption spectrum of a sample prepared with 7 layers thick NPLs and rinsed with ethanol after sensitization is also reported in Figure 1b. Although the peaks in its UV-VIS absorption spectra (indicated by a dotted line) were less structured, the sensitization still resulted in a redshift of the excitonic peaks confirming that is was due to the attachment of NPLs to the ZnO substrate.

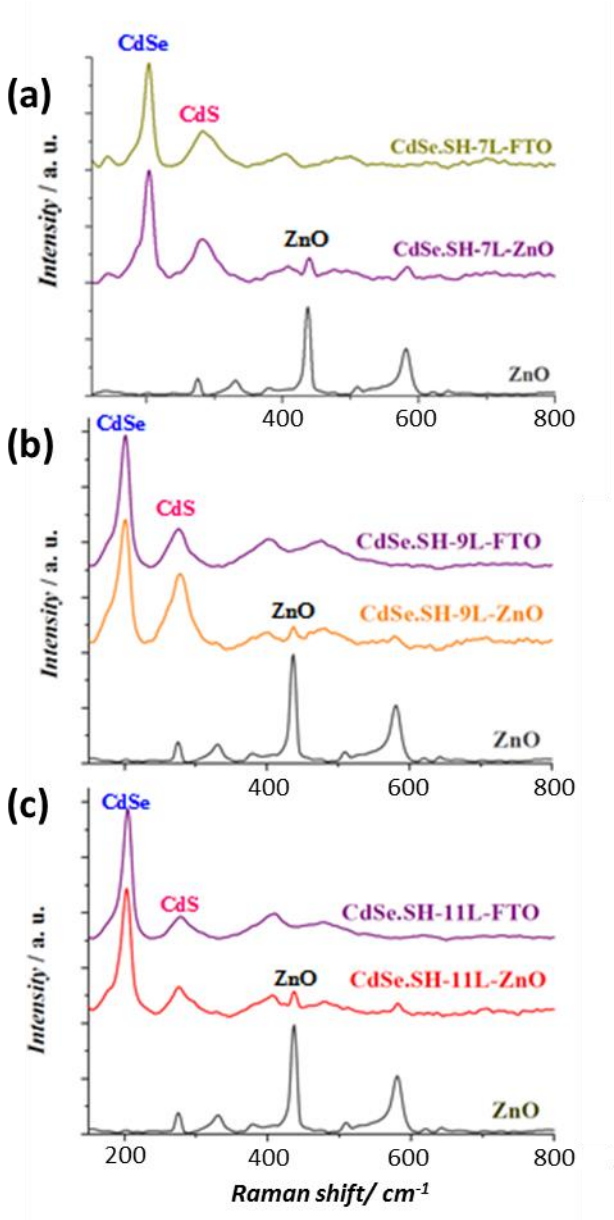

Figure 2. Raman spectra of a) 7, b) 9 and c) 11 layers thick CdSe.SH NPLs, of ZnO nanorod arrays sensitized by the same NPLs and of bare ZnO nanorod arrays.

In Figure 2, the Raman spectra of CdSe.SH NPLs of different thicknesses on FTO glasses are compared to the spectra of CdSe.SH-ZnO heterostructures and that of the bare ZnO NR arrays. The spectra of the CdSe.SH NPLs on the bare FTO-coated glass (represented as purple curves in Figure 2) features bands that correspond to the zinc blende phase of CdSe and of CdS. The reported spectra are globally very similar to previously published spectra of zinc blende CdSe/CdS core shell quantum dots. [23,24] The first band at around 200 cm^{-1} is attributed to the CdSe zinc blende longitudinal optical (LO) mode. Its broadening towards the

lower frequencies can be explained by the presence of interface and surface optical phonons, [23] as shown in Figure S7c (Supplementary Material). The band at around 280 cm^{-1} is attributed to the LO mode of the zinc blende phase of CdS, although redshifted compared to its bulk position near 300 cm^{-1}. This is due to the large strain that the single CdS layer suffers at the interface, as observed previously for CdSe/CdS core/shell QDs with a thin CdS shell. [21-24] The other modes observed for Raman shifts above 400 cm^{-1} correspond to overtones and mixed modes. [23,26]. In Figure 2, we can also observe the overlay of bands characteristic of the isolated NPLs and of the bare ZnO substrate, although the latter has a low intensity compared to the NPL bands. Therefore, only the highest intensity ZnO band is observable in these spectra at 438 cm^{-1}. In Figure 2, we did not observe a significant shift of the Raman bands of the semiconductor components after being linked together. In order to account for the changes that the CdSe.SH–ZnO interface formation induces in the Raman shifts, or the eventual formation of interface modes, a more refined measurement is needed and has been discussed in our previous work. [18]

When attached to TiO_2 nanorods, the dispersion of CdSe.SH NPLs of all thicknesses formed a homogeneously colored layer. The UV-VIS absorption spectra of these heterostructures are reported in Figure 3a, along with the UV-VIS absorption spectra of the bare NPLs for the sake of comparison. It can be observed for all NPL thicknesses that the NPL excitonic peaks are redshifted after the NPLs attachment to the oxide. However, they are far less structured in case of 7 layers thick NPLs than for 9 and 11 layers thick NPLs, suggesting that the original NPL structure is more distorted upon attachment to TiO_2 NRs if the nanocrystals are thinner.

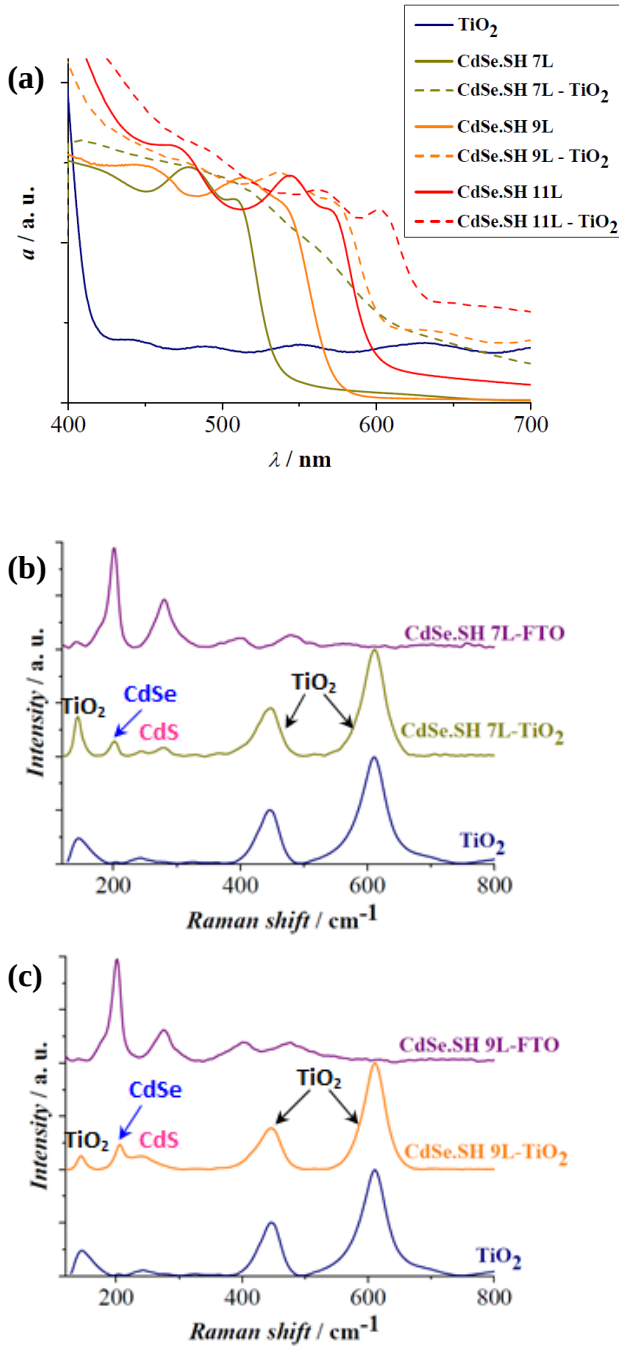

Figure 3. (a) UV-VIS absorption spectra of TiO_2 nanorod arrays and 7, 9 and 11 layers thick CdSe.SH NPLs in dispersion (indicated by green, orange and red full lines, respectively) and spectra after their attachment to TiO_2 nanorod arrays (indicated by dashed lines of the corresponding color). Raman spectra of (b) 7 and (c) 9 layers thick CdSe.SH NPLs, of TiO_2 nanorod arrays sensitized by the same NPLs and of bare TiO_2 nanorod arrays.

On the experimental Raman spectra of the CdSe.SH NPL-sensitized TiO_2 nanorod arrays (reported in Figure 3b,c and S8 (Supporting Information)), we can observe the overlay of the characteristic bands of the bare NPLs and of the bare TiO_2 substrate, although the latter has a

very high intensity compared to the NPL bands. Similarly to what was observed in the Raman spectra CdSe.SH–ZnO systems reported in Figure 1b, the NPL- and TiO_2-related bands observed in the Raman spectra of the CdSe.SH– TiO_2 heterostructures are found at the same Raman shift as in the Raman spectra of the bare NPLs and of the TiO_2 NR substrate, respectively.

3.2 Sensitization by OH^- functionalized NPL

In case of 7 L and 11 L thick NPLs, the ligand exchange reaction with OH^- resulted in the aggregation of the NPLs, and no homogeneous solution could be obtained. This observation is in agreement with a previous study in which it was demonstrated by FTIR that, unlike the OA^- to SH^- exchange, the OA^- to OH^- exchange on CdSe.QDs is only partial.[16] However, in case of 9 L thick NPLs, it was possible to obtain a homogeneous NPL dispersion after the biphasic OA^- to OH^- ligand exchange process. The UV-VIS absorption spectra of 9 L thick CdSe.OA and CdSe.OH NPLs are compared in Figure 4a. Only a small redshift of the excitonic peaks can be observed when the OA^- ligands are exchanged to OH^-.

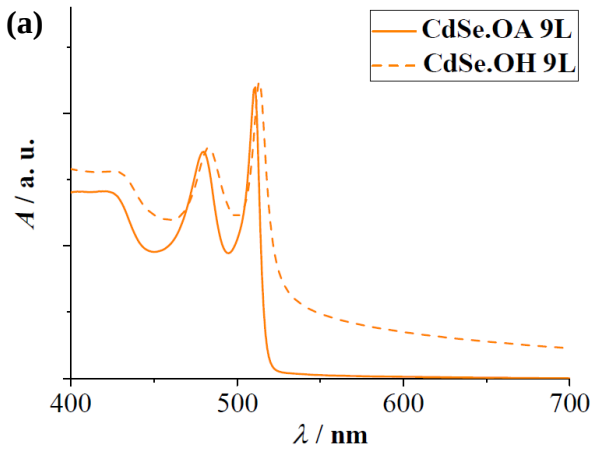

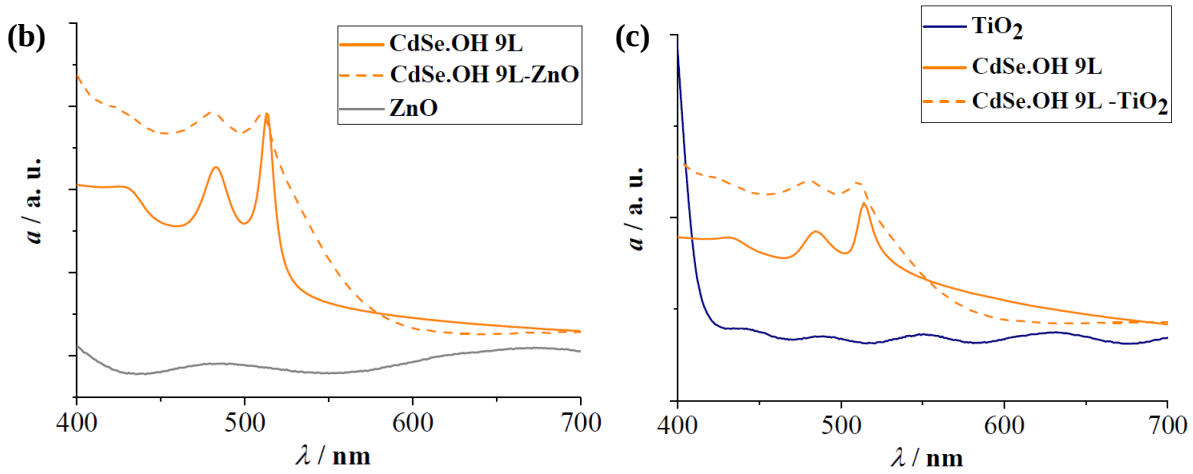

Figure 4. UV-VIS absorption spectra of (a) 9 layers thick CdSe NPLs before and after ligand exchange with OH^- (indicated by full and dotted lines, respectively). (b) ZnO NR arrays and 9 layers thick CdSe.OH NPLs in dispersion (indicated by orange full lines), as well as after attachment to ZnO NR arrays (indicated by orange dashed lines). (c) TiO_2 NR arrays and 9 layers thick CdSe.OH NPLs in dispersion (indicated by orange full lines) and after attachment to TiO_2 NR arrays (indicated by orange dashed lines)

It can be observed on the corresponding UV-VIS absorption spectra presented in Figures 4b and 4c that, after sensitization, the NPL excitonic peaks are only slightly blueshifted with respect to their position in the spectra of the bare NPLs, and this effect is enhanced when they are attached to TiO_2 NRs. This blueshift indicates a slight decrease in their thickness upon sensitization (presumably due to compressive strain along the thickness), in contrary to what was observed in case of CdSe.SH NPLs. According to Poisson's law, the compression of lattice constants in the *c* direction should result in the expansion of the lateral lattice parameter *a* and *b*. Indeed, this horizontal lattice expansion is manifested in the slight redshift of NPL-related CdSe LO Raman band, as reported in Figures 5a and 5b and Table S1. The ZnO and TiO_2 related bands remain in the same position as in the Raman spectra of the bare WBSC substrates.

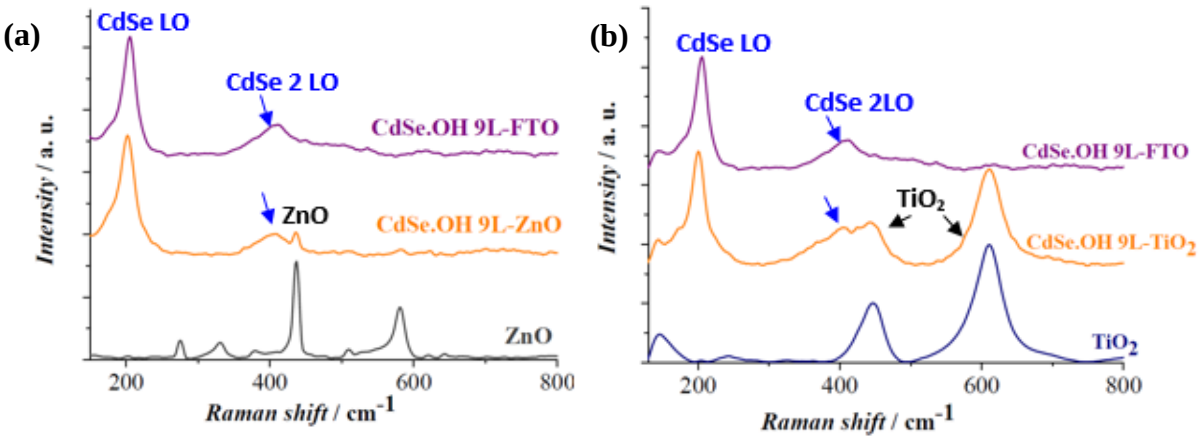

Figure 5. Raman spectra of (a) 9 layers thick CdSe.OH NPLs, of ZnO nanorod arrays sensitized by the same NPLs and of bare ZnO nanorod arrays and (b) 9 layers thick CdSe.OH NPLs, of TiO_2 nanorod arrays sensitized by the same NPLs and of bare TiO_2 nanorod arrays.

3.3. Sensitization by MPA functionalized NPLs

Similarly to SH^- ligand exchange reactions on CdSe NPLs, their passivation by MPA also resulted in the redshift of excitonic peaks, which became less structured than those of CdSe.OA NPLs, as reported in Figure 6. MPA ligands are known to link to the Cd-rich <100> NPL facets with their SH functional groups, it can be assumed that they also form a quasi-CdS shell on the CdSe NPLs. While the sensitization of WBSC substrates by CdSe.MPA NPLs was successful in case of 9 layers thick NPLs, 7 and 11 layers thick NPLs aggregated and did not form a homogeneous colored layer on the WBSC substrates. When attached to ZnO and TiO_2 NR arrays, the excitonic peaks of 9 layers thick CdSe.MPA NPLs did not significantly change their positions, they only became less structured, as illustrated in Figures 6b and 6c. This indicates that the sensitization-induced structural changes in the CdSe.MPA NPLs are less significant than in the CdSe.SH NPLs, which is intuitively explained by the fact that the MPA ligands increase the sensitizer-WBSC distance. The NPLs are thus not affected by strain caused by the lattice mismatch between the NPLs and the WBSC.

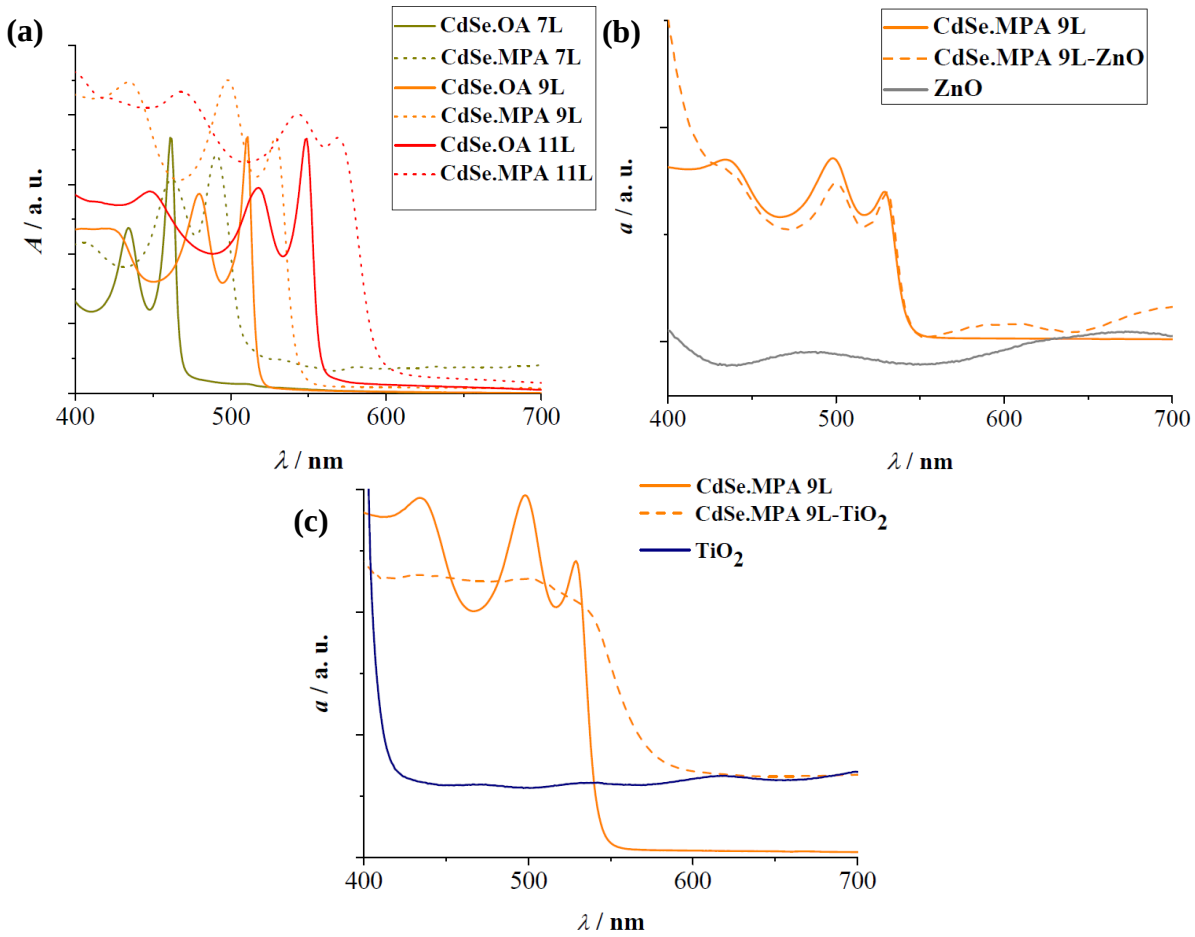

Figure 6. UV-VIS absorption spectra of (a) 7, 9 and 11 layers thick CdSe NPLs before and after ligand exchange with MPA (indicated by green, orange and red full and dotted lines, respectively). (b) ZnO NR arrays and 9 layers thick CdSe.MPA NPLs in dispersion (indicated by orange full lines) and after attachment to ZnO NR arrays (indicated by orange dashed lines). (c) TiO_2 NR arrays and 9 layers thick CdSe.MPA NPLs in dispersion (indicated by orange full lines) and after attachment to TiO_2 NR arrays (indicated by orange dashed lines)

The Raman spectra of the CdSe.MPA-ZnO and of the CdSe.MPA TiO_2 systems reported in Figures 7a and 7b, mainly features bands corresponding to its two components. A significant redshift of the CdSe LO bands can be observed after the NPLs are attached to the ZnO and TiO_2 nanorods, as reported in Table S2 (Supplementary Material), which suggests that in contrary to what we could observe from the UV-VIS absorption spectra reported in Figures 6b and 6c, the sensitization does alter the structure of CdSe.MPA NPLs.

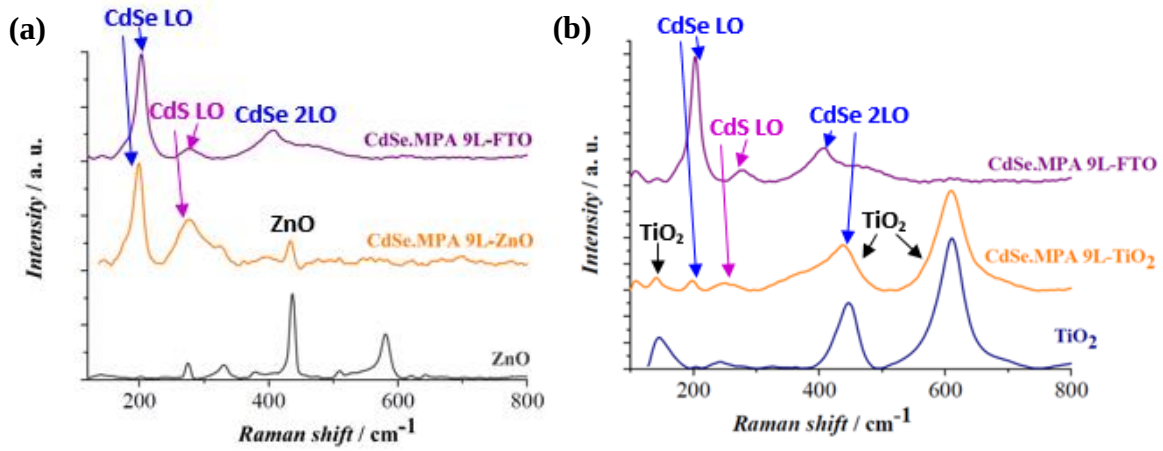

Figure 7. Raman spectra of (a) 9 layers thick CdSe.MPA NPLs, of ZnO NR arrays sensitized by the same NPLs and of bare ZnO NR arrays; of (b) 9 layers thick CdSe.MPA NPLs, of TiO_2 NR arrays sensitized by the same NPLs and of bare TiO_2 NR arrays.

3.4. Attachment of CdSe quantum dots to WBSCs

Ligand exchange reactions on CdSe QDs resulted in only a slight shift of excitonic peaks, as shown in Figure 8a. This is explained by the fact that the spherical quantum dots expose several different surfaces [27] on which the adhesion of ligands can be different. [28,29] Therefore, a large area of the QD surface can still remain passivated by OA after ligand exchange.

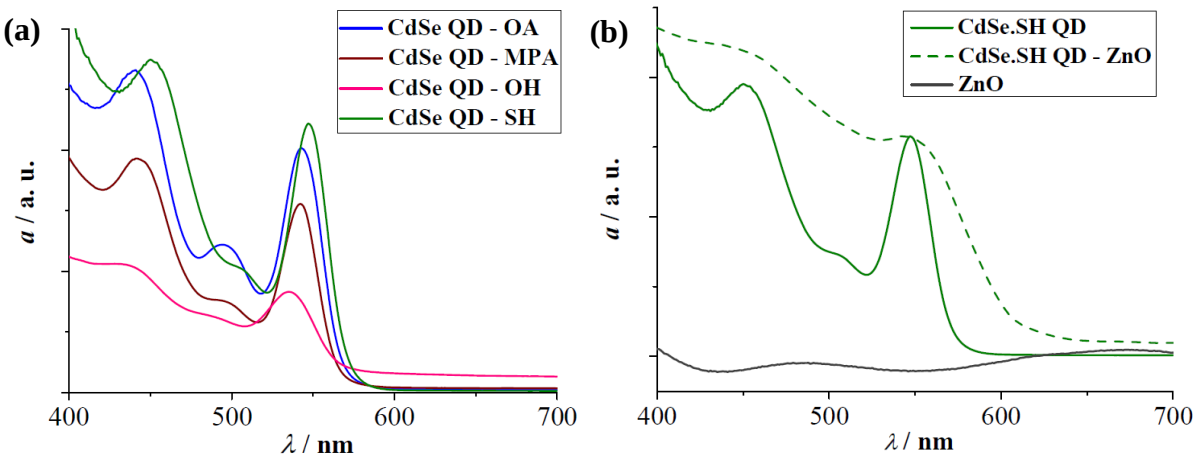

Figure 8. UV-VIS absorption spectra of (a) CdSe.OA QDs before and after ligand exchange with MPA^-, SH^- and OH^-; (b) ZnO NR arrays and CdSe.SH QDs in dispersion (indicated by green full lines) and after attachment to ZnO NR arrays (indicated by green dashed lines).

Among all ligand – WBSC combinations considered in this study, only the attachment of the CdSe.SH QDs to ZnO NR arrays was successful.[30] The sensitization using other linkers or a TiO_2 substrate resulted in the aggregation of QDs with an inhomogeneous coverage. The UV-VIS absorption spectrum of the CdSe.SH-ZnO system is compared to that of its components in Figure 8b. The QD excitonic peak positions are not significantly altered after sensitization, however the spectral bands become less structured. We can thus conclude that, in contrary to CdSe.SH NPLs, the quantum confinement effects in CdSe.SH QDs do not change dramatically after attachment to a WBSC surface, although their structural distortion is observable upon sensitization.

4. Conclusion

In summary, we have successfully functionalized the surface of CdSe nanocrystals (nanoplatelets of various thicknesses and spherical QDs) and linked them to ZnO and TiO_2 NR arrays via various ligands (SH^-, OH^- and MPA). The as-prepared nanocrystal-ligand-WBSC heterostructures have been thoroughly characterized by UV-VIS absorption and Raman spectroscopy. In some cases, CdSe.OH and CdSe.MPA nanocrystals aggregated on the WBSC nanorod arrays instead of forming a homogeneous layer. These sensitizations were thus regarded as unsuccessful, as these systems were not suitable for examining the effect of NPL thickness on the physical and chemical properties of these systems. On the other hand, the use of SH^- ligands with NPLs of various thicknesses, as well as QDs resulted in homogeneous CdSe nanocrystal films both on TiO_2 and ZnO nanorod arrays. The findings of the present work suggest that SH^- ligand can be regarded as versatile linker for the preparation of CdSe nanocrystal-sensitized solar cells. In particular, the CdSe.SH-ZnO systems have successfully been incorporated into solar cells, resulting in a maximum power conversion efficiency of 0.69%, as we have shown in Ref. [3].

Supplementary Material

Characterizations of ZnO nanorod arrays; Characterizations of TiO_2 nanorod arrays; TEM views of the CdSe nanoplatelets; Decomposition of experimental Raman spectra; Raman spectra of CdSe-SH NPLs; Raman shift of the CdSeOH NPLs LO band; Raman shift of CdSe MPA NPLs band.

Acknowledgements

This work was supported by the Région Ile-de-France in the framework of DIM Nano-K (Nanodot-PV project). Paris Sciences et Lettres (PSL) Research University is acknowledged for financial support (QuanDox project).

References

[1] C.J. Lin, S.N. Lin, J.H. Lai, Double-sided transparent photoanode of ZnO nanowire arrays sensitized by CdS and CdSe in photoelectrochemical cells for solar hydrogen production, Nanosci. Nanotechnol. Lett. 8 (2016) 961-964.

[2] G.M. Wang, X.Y. Yang, F. Qian, J.Z. Zhang, Y. Li, Double-sided CdS and CdSe quantum dot co-sensitized ZnO Nanowire Arrays for photoelectrochemical hydrogen generation, Nano Lett. 10 (2010) 1088-1092.

[3] A. Szemjonov, S. Ithurria, B. Dubertret, I. Ciofini, F. Labat, T. Pauporté, T, Ex situ and in situ sensitized quantum dot solar cells, Phys. Status Solidi B 254 (2017) 1600443.

[4] T. Takagahara, K. Takeda, Theory of quantum confinement effect on excitons in quantum dots of indirect-gap material, Phys. Rev. B 46 (1992) 15578-15581.

[5] W. Shockley, H.J. Queisser, Detailed balance limit of efficiency of P-N junction solar cells, J. Appl. Phys. 32 (1961) 510.

[6] A.G. Midgett, J.M. Luther, J.T. Stewart, D.K. Smith, L.A. Padilha, V.I. Klimov, A.J. Nozik, M.C. Beard, Size and composition dependent multiple exciton generation efficiency in PbS, PbSe, and PbS_xSe_{1-x} alloyed quantum dots, Nano Lett. 13 (2013) 3078- 3085.

[7] D. Vinoth Pandi, N. Muthukumarasamy, S. Agilan, D. Velauthapillai, CdSe quantum dots sensitized ZnO nanorods for solar cell application, Mater. Lett 223 (2018) 227-230

[8] F. Laatar, H. Moussa, H. Alem, L. Balan, E. Girot, G. Medjahdi, H. Ezzaouia, R. Schneider, CdSe nanorod/TiO_2 nanoparticle heterojunctions with enhanced solar- and visible-light photocatalytic activity, Beilstein J. Nanotechnol. 8 (2017) 2741-2752

[9] B. Guzeltur, P.L.H. Martine, Q.Zhang, Q. Xiong, H. Sun, X.W. Sun, A.O. Govorov, H.V. Demir, Excitonics of semiconductor quantum dots and wires for lighting and displays, Laser Photon. Rev. 8 (2014) 73-93.

[10] M. Li, M. Zhi, H. Zhu, W.Y. Wu, Q.H. Xu, M.H. Jhon, Y. Chan, Ultralow-threshold multiphoton-pumped lasing from colloidal nanoplatelets in solution, Nat. Commun. 6 (2015) 8513.

[11] A.W. Achtstein, A. Schliwa, M. Prudnikau Hardzei, M.V. Artemyev, C. Thomsen, U. Woggon, Electronic structure and exciton-phonon interaction in two-dimensional colloidal CdSe nanosheets, Nano Lett. 12 (2012) 3151- 3157.

[12] M.D. Tessier, C. Javaux, V. Maksimovic Loriette, B. Dubertret, Spectroscopy of single CdSe nanoplatelets, ACS Nano 6 (2012) 6751-6758.

[13] L.T. Kunneman, M.D. Tessier, H. Heuclin, B. Dubertret, Y. V Aulin, F.C. Grozema, J.M. Schins, L.D.A. Siebbeles, Bimolecular auger recombination of electron−hole pairs in two-dimensional CdSe and CdSe/CdZnS core/shell nanoplatelets, J. Phys. Chem. Lett. 4 (2013) 3574-3578.

[14] H.S. Kim, J.W. Lee, N. Yantara, P.P. Boix, S. Kulkarni, S. Mhaisalkar, M. Grätzel, N.G. Park NG. High efficiency solid-state sensitized solar cell-based on submicrometer rutile TiO_2 nanorod and $CH_3NH_3PbI_3$ perovskite sensitizer, Nano Lett. 13 (2013) 2412-2417.

[15] S. Ithurria, G. Bousquet, B. Dubertret, Continuous transition from 3D to 1D confinement observed during the formation of CdSe nanoplatelets., J. Am. Chem. Soc. 133 (2011) 3070-3077.

[16] A. Nag, M.V. Kovalenko, J.S. Lee, W. Liu, B. Spokoyny, D. Talapin, Metal-free inorganic ligands for colloidal nanocrystals : S^{2-} , HS^- , Te^{2-}, HTe^-, TeS_3^{2-}, OH^- and NH_2^- as surface ligands, J. Am. Chem. Soc. 133 (2011) 10612-10620.

[17] A. Szemjonov, T. Pauporté, S. Ithurria, N. Lequeux, B. Dubertret, I. Ciofini, F. Labat, Ligand-stabilized CdSe nanoplatelet hybrid structures with tailored geometric and electronic properties. New insights from theory, RSC Adv. 4 (2014) 55980-55989.

[18] A. Szemjonov, T. Pauporté, S. Ithurria, S. Pedetti, N. Lequeux, B. Dubertret, I. Ciofini, F. Labat, Towards the modeling of quantum-dot sensitized solar cells: From structural and vibrational features to electron injection through lattice-mismatched interfaces, J. Mater. Chem. A 4 (2016) 13081-13092.

[19] A. Szemjonov, T. Pauporté, I. Ciofini, F. Labat, Bulk and surface properties investigation of CdSe: insights from theory, Phys. Chem. Chem. Phys. 16 (2014) 23251-23259.

[20] S. Flamee, M. Cirillo, S. Abe, K. De Nolf, R. Gomes, T. Aubert, Z. Hens, High yield and high solid loading synthesis of metal selenide nanocrystals, Chem. Mater. 25 (2013) 2476-2483.
[21] Z. Pan, I. Mora-Seró, Q. Shen, H. Zhang, Y. Li, K. Zhao, J. Wang, X. Zhong, J. Bisquert J. High-efficiency "green" quantum dot solar cells. J. Am. Chem. Soc. 136 (2014) 9203-9210.
[22] S. Ithurria, M.D. Tessier, B. Mahler, R. Lobo, B. Dubertret, A.L. Efros, Colloidal nanoplatelets with two-dimensional electronic structure, Nat. Mater. 10 (2011) 936-941.
[23] N. Tschirne, H. Lange, A. Schliwa, A. Biermann, C. Thomsen, C.K. Lambert, R. Gomes R, Z. Hens, Interfacial alloying in CdSe/CdS heteronanocrystals: A Raman spectroscopy analysis, Chem. Mater. 24 (2012) 311-318.
[24] C. Lin, K. Gong, D.F. Kelley, A.M. Kelley, Electron-phonon coupling in CdSe/CdS core/shell quantum dots, ACS Nano 9 (2015) 8131-8141.
[25] V.M. Dzhagan, M.Y. Valakh, A.G. Milekhin, N.A. Yeryukov, D. Zahn, E. Cassette, T. Pons, B. Dubertret, Raman- and IR-active phonons in CdSe/CdS core/shell nanocrystals in the presence of interface alloying and strain, J. Phys. Chem. C 117 (2013) 18225-18233.
[26] L. Lu, X.L. Xu, W.T. Liang, H.F. Lu, Raman analysis of CdSe/CdS core-shell quantum dots with different CdS shell thicknesses, J. Phys. Condens. Matter 19 (2007) 406221.
[27] Y.Yang, Y.H. Wu, K.R. Williams, Y.C. Cao, Synthesis of CdSe and CdTe nanocrystals without precursor injection, Angew. Chemie 44 (2005) 6712-6715.
[28] Z. Peng, X. Peng, Mechanisms of the shape evolution of CdSe nanocrystals, J. Am. Chem. Soc. 123 (2001) 1389-1395.
[29] J.S. Owen, J. Park, P.E. Trudeau, A.P. Alivisatos, Reaction chemistry and ligand exchange at cadmium-selenide nanocrystal surfaces, J. Am. Chem. Soc. 130 (2008) 12279-12281.
[30] C. Badre, P. Dubot , D. Lincot T. Pauporté, M. Turmine, Effects of nanorod structure and conformation of fatty acid self assembled layers on superhydrophobicity of zinc oxide surfaces, J. Colloids Interf. Science, 316 (2007) 233-237.